12th International Symposium on Turbulence and Shear Flow Phenomena (TSFP12)
Osaka, Japan, July 19–22, 2022

EFFECT OF INCOMING BOUNDARY LAYER CHARACTERISTICS ON AN AIR LAYER WITHIN A LIQUID TURBULENT BOUNDARY LAYER

Lina Nikolaidou
Department of Process and Energy
Delft University of Technology
Mekelweg 2, 2628 CD Delft. Netherlands
M.Nikolaidou@tudelft.nl

Angeliki Laskari
Department of Process and Energy
Delft University of Technology
Mekelweg 2, 2628 CD Delft, Netherlands
A.Laskari@tudelft.nl

Christian Poelma
Department of Process and Energy
Delft University of Technology
Mekelweg 2, 2628 CD Delft, Netherlands
C.Poelma@tudelft.nl

Tom van Terwisga
Department of Maritime and Transport Technology
Delft University of Technology/
Maritime Research Institute of the Netherlands (MARIN)
Mekelweg 2, 2628 CD Delft, Netherlands
T.v.Terwisga@marin.nl

ABSTRACT

An air layer within a liquid turbulent boundary layer (TBL) is formed by controlled air injection underneath a flat plate. The incoming boundary layer as well as the flow around the air layer were measured with planar particle image velocimetry (PIV). The effect of different incoming liquid flow characteristics on the air layer geometry is investigated by varying both the freestream velocity and the streamwise development length of the TBL. The latter was realized through changing the position of the air injection along the length of the water tunnel facility. Increasing the freestream velocity resulted in an increase of the air layer length, while its maximum thickness remained relatively unaltered. An increase in the TBL development length, had a similarly marginal effect on the resulting maximum air layer thickness but led to a shorter air layer length. The latter could be attributed to a decrease in local mean velocity due to the TBL growth, reflected in a decrease of the air layer to boundary layer thickness ratio (from 0.27 to 0.17). The results of this study are expected to provide insight on the design conditions of an air layer drag reduction system installed in the hull of a ship.

MOTIVATION

Friction drag accounts on average for approximately 70% of the overall resistance of a ship (Larsson & Raven, 2010), and thus a large part of a typical ship's propulsive power is required to overcome it. To reduce this drag air layer lubrication techniques have been proposed and investigated over the past years, among other methods. These techniques could lead to fuel cost savings and a lower environmental impact. While drag reduction measurements using a variety of injectors and flow conditions have been performed by different research groups to date, few scaling laws able to collapse the data are available. Past studies, depending on the capabilities of the experimental facilities used, investigated the effect of the freestream velocity and/or the incoming liquid boundary layer thickness on the air layer flow in different ways. In the study of Zverkhovskyi (2014), the incoming liquid TBL thickness was varied via changing the air injection position. Only marginal differences in the resulting air layer thickness and length were observed, although the interface was shown to be more energetic for larger development lengths; however, no detailed study of the liquid flow field around the layer was performed. In the same study, the effect freestream velocity was also investigated. An increase in the air layer length with increasing freestream velocities was observed, with the maximum air layer length (for a specific freestream velocity) occurring at approximately a half gravity wave length (Zverkhovskyi, 2014). In the study of Pearce *et al.* (2015), the incoming liquid TBL thickness was varied by artificial thickening (or thinning) at the water tunnel inlet, and the effect of different freestream velocities was also examined. In contrast to the results from Zverkhovskyi (2014), an increase in the freestream velocity led to a shorter air cavity while the opposite was true for a decrease of the boundary layer thickness. The authors attributed the latter to the lower kinetic energy at the air-water interface, although no turbulence profile measurements were performed to further support this assumption.

Much fewer studies are available on the effect of incoming boundary layer characteristics on the air layer thickness. This is possibly due to the difficulties that such a measurement entails. Instead of measuring the air layer thickness directly, many studies define a nominal air thickness $t_{air} = \frac{Q_{air}}{BU_\infty}$ with Q_{air} the air flow rate, B the injector span and U_∞ the liquid freestream velocity (Elbing *et al.* (2008, 2013); Peifer *et al.* (2020)). However it is still unclear how this relates to the physical air layer thickness.

In the above studies, a cavitator or a backward facing step (BFS) was used upstream of the air injection. In the absence of such inserts (which is the desirable configuration for full-scale applications), the effect of the upstream conditions on the characteristics of the resulting air layer is expected to be stronger. Nonetheless, experiments in such a geometry for a bubble drag reduction regime (BDR) showed that a doubling of the boundary layer thickness at the injection position had a negligible effect on the resulting drag (Elbing *et al.*, 2008); this effect was not investigated in the case of an air layer however.

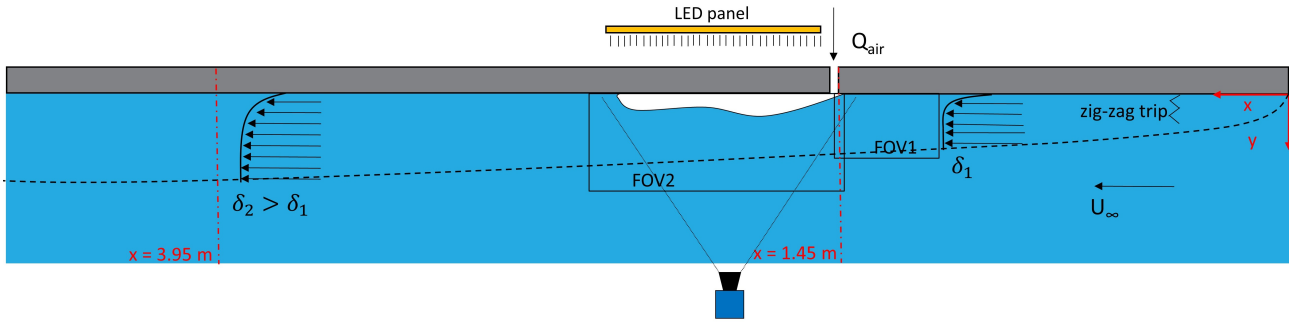

Figure 1: Schematic representation of the setup. The two different injection positions are indicated in red. FOV1 is the field of view for the incoming boundary layer and FOV2 for the flow around the air layer. The measuring system is shown for position x = 1.45 m. In the case of the measurement in position x = 3.95 m the entire measurement system moves downstream. Flow is from right to left.

Table 1: Summary of the incoming boundary layer properties for two different injection positions.

Pos.	x (m)	U_∞ (m/s)	Re_x	Re_θ	Re_τ	θ (mm)
1	1.45	0.68	993250	2970	1532	4.13
1	1.45	0.77	1118530	3677	1688	4.41
1	1.45	0.86	1261500	3614	1409	4.02
1	1.45	0.92	1363000	4781	2098	4.93
2	3.95	0.71	2808450	5343	3481	7.43
2	3.95	0.80	3161580	7462	4495	8.9
2	3.95	0.89	3436500	7254	3352	7.76
2	3.95	0.96	3713000	8025	3636	7.97

In the current study, we aim to revisit some of these questions, specifically targeting the effect of the incoming boundary layer characteristics on the geometry of the air layer developed downstream of the air injection, without the use of a cavitator or a BFS. This is achieved by varying both the freestream velocity and the streamwise development length of the liquid boundary layer, resulting in a large range of Reynolds numbers for the incoming flow. The effect of those changes in the resulting air layer geometry are subsequently evaluated.

EXPERIMENTAL SETUP

Experiments were performed in the water tunnel of the Laboratory for Aero & Hydrodynamics of the Delft University of Technology. The test section of the tunnel has a cross-sectional area of 60 $\times$ 60 cm^2 and a length of 5 m. The open surface of the water tunnel was covered with two identical flat plates, each 2.485 m long, tightly placed one after the other. The water depth was d = 58 cm. One of the plates was fitted with a slot type air injector, spanning the central 58 cm of the plate width. The length of the slot was 4 mm. Both plates were equipped with side fences to prevent the air from escaping through the sides. Compressed air was injected from the top side of the plate through two manifolds and dispersed over the width of the slot. The air flow rate, Q_{air}, was manually controlled with a valve and measured with a rotameter. A constant air flow rate of 42 l/min was used which resulted in a stable air layer for all cases tested here (see also Nikolaidou *et al.*, 2021). The flow was tripped with a 0.5 mm thick zig-zag trip located 8 cm downstream of the start of the flat plate. The corresponding Re_θ at the tripping location varied from 150 to 190 based on the Blasius's solution for a laminar boundary layer.

The incoming boundary layer upstream of the air injection, as well as its development around the air cavity, were measured simultaneously with planar (2D-2C) PIV using two high-resolution LaVision LX pro (16 MegaPixel), 12-bit cameras. The acquisition frequency was 0.7 Hz and 1600 statistically independent images were recorded for each dataset. The laser sheet was introduced from the bottom creating a thin sheet ($\sim$ 1 mm) in a streamwise–wall-normal (x-y) plane at the tunnel's mid-span. The optical magnification was approximately 12 px/mm for the larger (downstream) FoV and 27 px/mm for the smaller (upstream) one, resulting in a spatial resolution of the velocity field (based on the final interrogation window size) of 2 mm and 0.88 mm respectively. Finally, a LaVision's Imager sCMOS CLHS camera was used to image the air layers in a streamwise-spanwise plane. The image acquisition rate was 2 Hz, allowing independent snapshots. The field of view was approximately 700 x 600 mm^2 and the magnification approximately 3.6 px/mm in both directions. A sketch of the experimental setup can be seen in figure 1.

The experimental campaign included both a variation of the air injector position (in x, with x=0 at the origin of the boundary layer) and the freestream velocity. The tested freestream velocities ranged from 0.68 m/s to 0.96 m/s with a Reynolds number based on the water depth, Re_d ranging from 3.94 $\times$ 10^5 to 5.45 $\times$ 10^5. The air injector was positioned 0.45 m and 1.95 m from the start of the test section. However, as indicated by previous measurements at the water tunnel (Harleman *et al.* (2011)), the boundary layer development starts in the contraction region prior to the test section (approximately 1 m upstream). This is also considered in the current measurements. In each position, apart from measurements with an air layer present, single phase flow measurements (without the air layer) were performed as well to serve as a reference case. In the current paper, the incoming TBL results are presented for the one phase flow case only. These are summarized in table 1. It must be noted that the incoming boundary layer experiences the presence of the air layer and results of the two phase flow case are expected to show a difference as seen in Anand (2021).

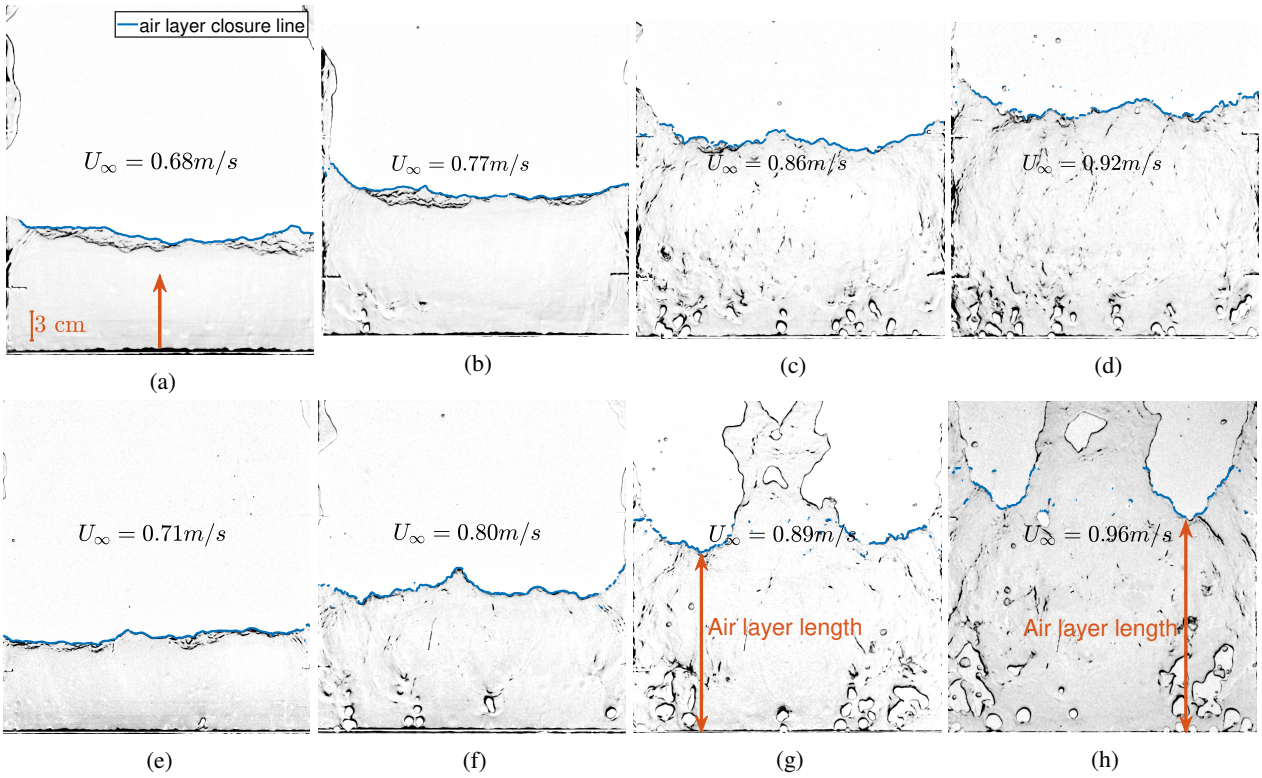

Figure 2: Characteristic air layer images for different air injection positions and freestream velocities. For the shorter development length of $x = 1.45$ m (a)-(d) and the larger development length of $x = 3.95$ m (e)-(h). Flow is from down up.

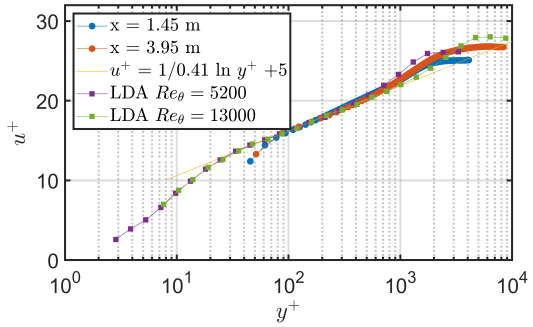

Figure 3: Double mean streamise velocity profiles of the incoming boundary layer for the two different air injection positions compared with LDA data from De Graaff & Eaton (2000).

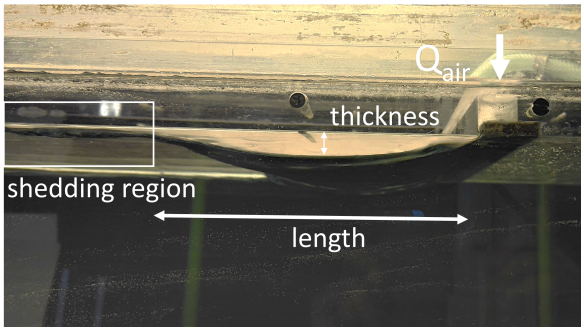

Figure 4: Side view of the air layer. Flow is from right to left.

RESULTS

First a characterization of the incoming TBL was performed for the two different air injection positions (x = 3.95 m and x = 1.45 m). Mean velocity profiles and mean normal and shear stresses were computed but only the mean velocities are discussed in this paper. The mean velocity profiles were spatially averaged over the length of the field of view (FOV1 in figure 1) in the absence of strong streamwise gradients. The double average profiles in the case of the higher freestream velocity considered can be seen in figure 3. It must be noted that FOV1 was considerably larger than the boundary layer thickness (larger than $1.5\delta_{99}$). Due to imperfections of the setup and the water tunnel itself, the freestream region was more noisy than expected and a large extent of FOV1 & FOV2 in the wall-normal direction provided a clearer picture of the freestream region.

The boundary layer thickness was defined as the wall normal distance where the velocity is 99% of the freestream velocity U_∞. The freestream velocity U_∞ and δ_{99} were then determined iteratively with U_∞ defined as the mean of all data points with $y > \delta_{99}$. The friction velocity was determined with the Clauser chart method (Clauser (1956)). The computed freestream velocities indicated a increase of 4% from the shorter to the longer development length in the absence of a slopping bed in the bottom of the tunnel (see also table 1). The incoming boundary layer thickness for the larger development length ($\delta_{99} = 96$ mm) was approximately double in size compared to the smaller development length ($\delta_{99} = 53$ mm).

Next the air layer characteristics (length L_{air} and thickness t_{air}) were computed. In this case t_{air} is the actually measured one. The air layer length was determined from the images of the down-up camera (see camera in figure 1). An edge detection algorithm was employed to locate the closure line of the air layer in each image (figure 2). This included a median filtering of the image, background normalization, increase of the contract. The grayscale image was then binarized based on

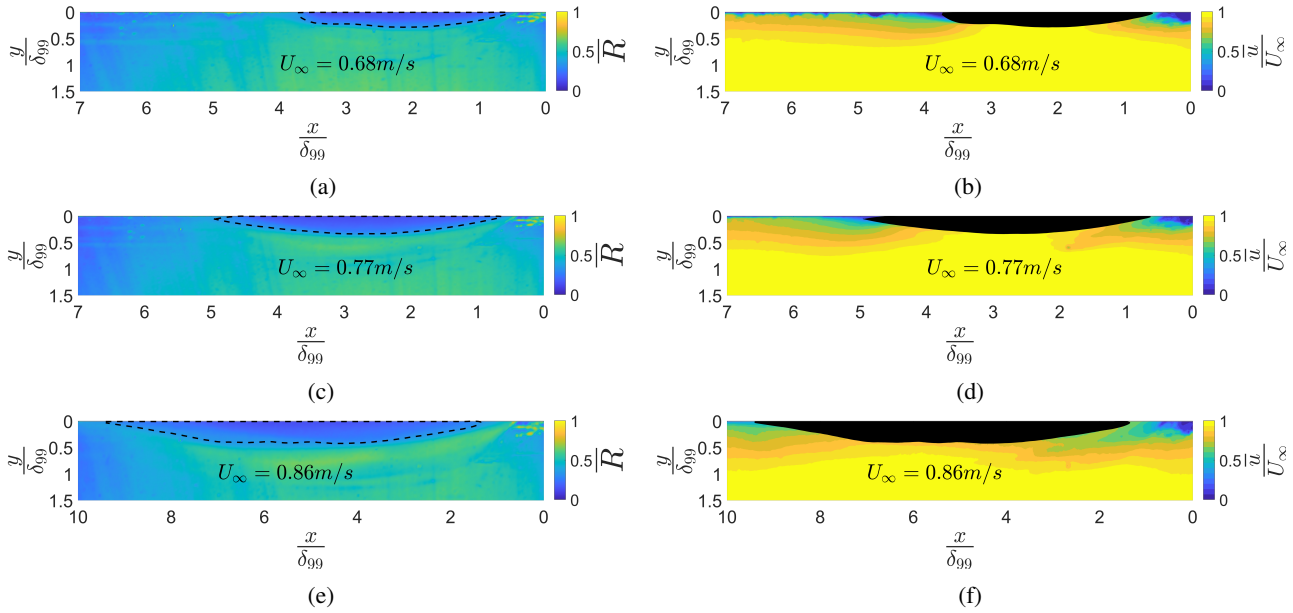

Figure 5: Mean correlation map for the shorter streamwise development length (a),(c),(e). The black dotted line indicates the edge of the air layer. Contours of the mean streamwise velocity in the same position (b),(d),(f). The air layer is in black.

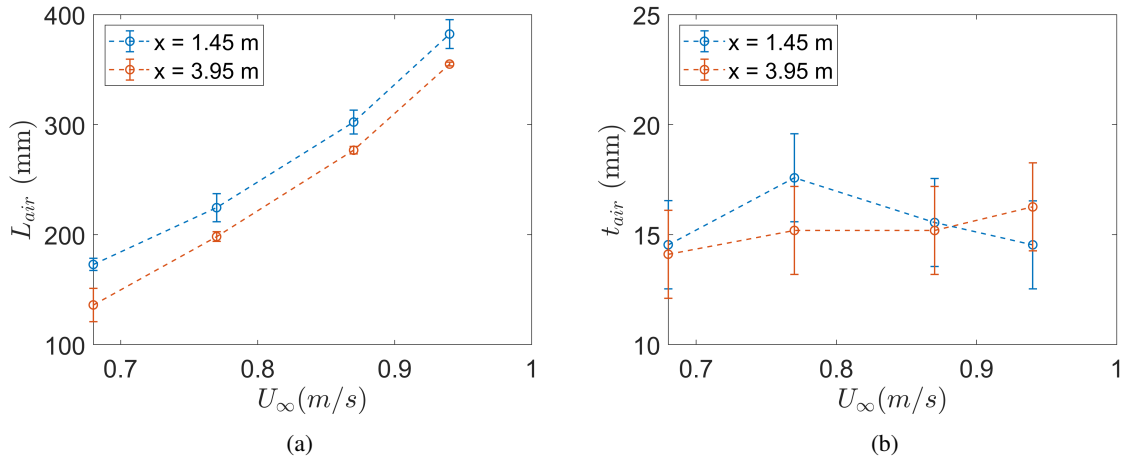

Figure 6: Air layer length (a) and maximum air layer thickness (b) in different freestream velocities and two streamwise development lengths.

a threshold and the air closure line was detected (blue lines in figure 2). At each instantaneous image, L_{air} was estimated as the shortest streamwise distance of the identified closure line from the injector. This was done to ensure that only the spanwise homogeneous part of the air layer is considered (indicated as "length" in figure 4). At higher velocities and for the larger development length, air leakage was observed in the form of three elongated air stripes creating an inhomogeneous distribution in the spanwise direction (see also figures 2g and 2h). The length of these air strips is not considered in the aforementioned definition since it is still unclear if these regions contribute to drag reduction. Furthermore, they could not be quantified with the present set-up.

The thickness t_{air} was determined from the mean correlation value $\overline{R}$ of the particle image pairs (figure 5). More specifically, a noticeable decrease of the correlation value was observed inside the air layer because of the absence of seeding particles in the air phase. Subsequent appropriate thresholding and image processing of the mean correlation maps allowed the determination of the mean air water interface and its maximum thickness (at the apex of the concave interface) for all conditions. Another way of determining the air layer thickness from PIV images was proposed by Anand (2021), where the air-water interface is estimated at each time instance, using the instantaneous instead of the mean correlation maps. It must be noted that an estimate of the L_{air} could be also obtained by the mean correlation map in a similar manner as t_{air} was determined. However, difficulties pertaining to the unsteady character of the closure region of the air layer made the detection of L_{air} through the PIV images challenging, especially for the higher freestream velocities. As a result the air layer length L_{air} was determined solely based on the imaging camera.

Once the air layer geometry is determined, it is possible to get an idea of the mean flow around the air layer (figures 5d,5e,5f). As the boundary layer approaches the air layer it experiences consecutively an adverse, a favorable and then again an adverse pressure gradient. The boundary layer is thinnest

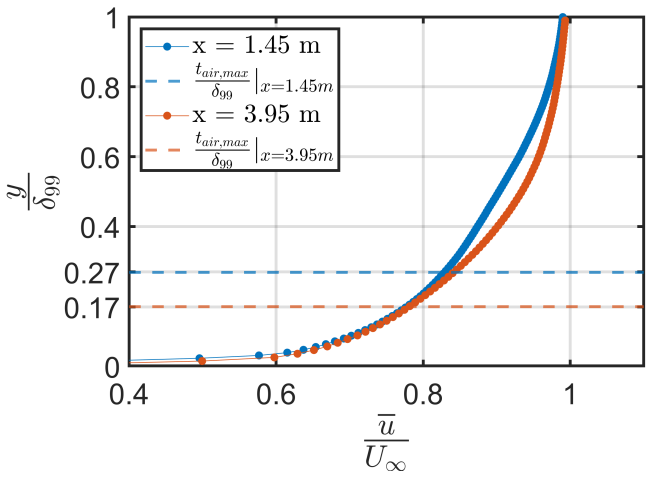

Figure 7: Mean streamwise velocity profile in the case of the higher velocity for the shorter (x = 1.45 m) and the longer (x = 3.95 m) streamwise developing length.

approximately at the apex of the air layer. Similar observations were also documented in Anand (2021). In the case of increasing freestream velocity, the magnitude of the alternating pressure gradients is qualitatively smaller. Further analysis of the liquid flow around the air layer is ongoing.

The effect of the different freestream velocities and air injection positions on the air layer characteristics can be seen in figure 6. Increasing U_∞ resulted in a marked increase of L_{air}, a trend qualitatively matched for the two different TBL development lengths; an increase in the latter led to a consistently shorter L_{air} for all velocities although that effect was much weaker (figure 6a). The variation of t_{air} in response to changes in both U_∞ and development length was within the experimental uncertainty of 2 mm (owing to the sensitivity of the detection method and the PIV resolution) and thus no measurable effect of either parameter could be identified (figure 6b).

DISCUSSION AND CONCLUSIONS

The aforementioned observations indicate that both the incoming boundary layer characteristics and the freestream velocity affect the air layer geometry. Larger air layer lengths were found for larger freestream velocities. This effect of the freestream velocity on the air layer length is intuitively easier to grasp; in order to better understand the effect of the TBL development length however, it is instructive to consider the thickness ratio between the air layer and the TBL $\frac{t_{air}}{\delta_{99}}$. For both injector locations, the air layer is significantly thinner than the TBL - its maximum reaching just the end of the log ($\frac{t_{air}}{\delta_{99}} \approx 0.17$) and the lower wake region ($\frac{t_{air}}{\delta_{99}} \approx 0.27$) for the larger development length (x = 3.95 m) and the shorter one (x = 1.45 m), respectively. It then follows that the local mean velocity of the TBL at the height of the air layer would decrease as the TBL develops downstream (from 0.76 m/s to 0.75 m/s approximately for the higher U_∞ shown in figure 7). The resulting decrease in the air layer length is then in line with the observed speed dependency discussed above. This indicates that, as far as the mean characteristics of the air layer are concerned - and for the range of conditions tested here - the liquid velocity in the vicinity of the air layer is the most prominent influence. In the study of Zverkhovskyi (2014), the freestream velocity rather than the local one was identified to have the bigger effect on the air cavity length. However in the aforementioned study the thickness ratio $\frac{t_{air}}{\delta_{99}}$ under consideration was significantly large and as a result the local velocity at the air thickness height t_{air} in this case would be closer to the freestream velocity in comparison to our case here. Apart from the effect of the local velocity to the air layer, potential effects due to the different structuring of the TBL as it develops downstream are much more difficult to identify in the current campaign but they are expected to exert a larger influence on the instantaneous rather than average characteristics of the air liquid interface (such as the different topology observed in figure 2).

In conclusion, increasing the freestream velocity resulted in an increase of the air layer length, while its maximum thickness remained relatively unaltered. An increase in the TBL development length, had a similarly marginal effect on the resulting maximum air layer thickness but led to a shorter air layer length. Consideration of the thickness ratio between the air layer and the TBL reveals that the liquid velocity in the vicinity of the air layer has the bigger effect on the air layer length. In the real case scenario of an air layer beneath the hull of a ship, the air layer thickness would be a small fraction of the the incoming boundary layer (~ 1) and thus considerations in this study could help in the air injection position along the hull.

ACKNOWLEDGEMENTS

This work is part of the public-private research program "Water Quality in Maritime Hydrodynamics" (AQUA) project P17-07. The support by the Netherlands Organisation for Scientific Research (NWO) Domain Applied and Engineering Sciences, and project partners is gratefully acknowledged.

REFERENCES

Anand, Abhirath 2021 Experimental investigation of influence of an air cavity on a turbulent boundary layer using PIV. Master's thesis, TU Delft, the Netherlands.

Clauser, Francis H 1956 The turbulent boundary layer. *Advances in applied mechanics* **4**, 1–51.

De Graaff, David B & Eaton, John K 2000 Reynolds-number scaling of the flat-plate turbulent boundary layer. *Journal of Fluid Mechanics* **422**, 319–346.

Elbing, Brian R, Mäkiharju, Simo, Wiggins, Andrew, Perlin, Marc, Dowling, David R & Ceccio, Steven L 2013 On the

scaling of air layer drag reduction. *Journal of fluid mechanics* **717**, 484–513.

Elbing, Brian R, Winkel, Eric S, Lay, Keary A, Ceccio, Steven L, Dowling, David R & Perlin, Marc 2008 Bubble-induced skin-friction drag reduction and the abrupt transition to air-layer drag reduction. *Journal of Fluid Mechanics* **612**, 201–236.

Harleman, MJW, Delfos, R, Van Terwisga, TJC & Westerweel, J 2011 Dispersion of bubbles in fully developed channel flow. In *Journal of Physics: Conference Series*, , vol. 318, p. 052007. IOP Publishing.

Larsson, Lars & Raven, Hoyte C. 2010 Ship Resistance and Flow. *The Principles of Naval Architecture Series, ISBN: 978-0-939773-76-3* .

Nikolaidou, L., Laskari, A., van Terwisga. T. & Poelma, C. 2021 On the characteristics of air layer regimes. In *11th International Symposium on Cavitation 2021 (CAV2021)*, pp. 386–3914. The Society of Naval Architects of Korea.

Pearce, BW, Brandner, PA & Foster, SJ 2015 Ventilated cavity flow over a backward-facing step. In *Journal of Physics: Conference Series*, , vol. 656, p. 012164.

Peifer, Bradley C, Callahan-Dudley, Christopher & Mäkiharju, Simo A 2020 Air layer on superhydrophobic surface for frictional drag reduction. *Journal of Ship Research* **64** (2).

Zverkhovskyi, Oleksandr 2014 Ship drag reduction by air cavities. PhD thesis, TU Delft, the Netherlands.